THz time domain spectroscopy of doped poly *p*-phenylene vinylene (MEH-PPV)

Tae-In Jeon[a], Keun-Ju Kim[a], A.K. Mukherjee[b] and Reghu Menon[b]

[a]Korea Maritime University, Division of Electrical and Electronics Engineering, Busan 606-791, South Korea
[b]Department of Physics, Indian Institute of Science, Bangalore 560012, India

Abstract

An optoelectronic contactless method by THz time domain spectroscopy (THz-TDS, in the frequency range 0.5–3.0 THz) has been used to measure the absorption, dispersion, and reflectance of $FeCl_3$-doped poly(2-methoxy-5-(2′-ethyl)hexyloxy-*p*-phenylene vinylene) [MEH-PPV] film. The measured data fit well to Lorentz oscillator (LO) model indicating that free carriers are negligible though the system is fairly conducting ($\sim$0.1 S/cm) at room temperature. The large value of the coupling constant ($\Omega_{p1}/2\pi$ = 14.7 THz) in LO model indicates that intra-chain localization of carriers is rather strong and the inter-chain transport is quite weak.

Keywords: Time-resolved fast spectroscopy; Conductivity; Terahertz

Article Outline

1. Introduction

The conducting and semiconducting properties of conjugated polymers have attracted considerable attention over the past decade due to several applications in polymer electronics [1]. A systematic technique to accurately measure the charge transport parameters, and to understand the carrier dynamics in these disordered quasi-one-dimensional systems is yet to be fully developed [2] and [3]. Nevertheless, the recent THz time domain spectroscopy (THz-TDS) [4] and [5] in conducting polypyrrole (PPy-PF_6) [6] and poly-3-methylthiophene (P3MeT-PF_6) [7] has shown that the charge transport parameters like mobility, carrier density, scattering time, etc., can be directly determined by this experimental method. Since poly-*p*-phenylene vinylene (PPV) derivatives [8] are widely used in light emitting diodes, solar cells, etc.; it is of considerable importance to investigate the charge transport parameters by THz-TDS. The advantage in THz-TDS is that the absorption and dispersion of the sample can be measured directly, and this is expected to give much more accurate values of the charge transport parameters, with respect to other methods [9].

2. Experimental

In general, the electrical and optical properties of semiconductors are governed by the response of mobile charge carriers and its interaction with the surroundings [1]. In simple Drude model, the two parameters that characterize the non-interactive charge carriers are plasma frequency (ω_p) and relaxation rate Γ (=1/τ), where τ is the average collision time between the carriers. Since, both parameters are usually in the THz range, a probe that can investigate the system in the THz frequency range is highly desirable, as in the case of THz-TDS. MEH-PPV was synthesized by Wessling polyelectrolyte precursor route [10]. The measurement was made on free-standing films (thickness $\cong$17 μm) of MEH-PPV doped by $FeCl_3$ prepared by solution cast method.

Reflectivity and complex conductivity are determined from the measured power absorption and index of refraction, from 0.5 to 3 THz. Because the dc conductivity ($\sim$0.1 S/cm) of MEH-PPV/$FeCl_3$ was much less than that of P3MeT-PF_6 samples (7.5 S/cm), in which THz-TDS measurement has already been reported [7], the frequency dependence of conductivity in former has shown a marked difference. The measured data by THz-TDS for MEH-PPV/$FeCl_3$ could be fitted only to Lorentz oscillator (LO) model [11], whereas Drude model [12] and localization-modified Drude model [13] were quite appropriate for metallic PPy-PF_6 ($\sim$215 S/cm) and for slightly insulating P3MeT-PF_6 ($\sim$7.5 S/cm), respectively.

The basic idea [14] involved in THz-TDS is to measure the change of amplitude and phase shift of freely propagating electromagnetic pulses after it has passed through the polymer film, and then compare that with respect to the THz pulses in absence of sample. The frequency dependent absorption and refractive index are obtained by the analysis of the

respective numerical Fourier transforms. The reference pulse with no sample in place is shown in Fig. 1(a). The THz pulse freely propagated through air. The signal to noise ratio is around 10,000:1 which is large enough for the analysis. The THz pulse after passing through the $FeCl_3$ doped MEH-PPV film, which has 17 μm thickness, is shown in Fig. 1(b), in which the amplitude shows a very small drop. The normalized amplitude spectrum of THz pulse in the same frequency domain is shown in Fig. 1(c). Although there is very small difference between the line shapes of two pulses in time domain, the phase difference between the two pulses in frequency domain is clear to make a good estimate of refractive index.

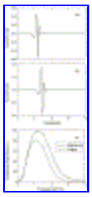

(34K)

Fig. 1. (a) Measured reference input THz pulse (through air) in time domain. (b) Measured output THz pulse transmitted through the MEH-PPV film doped by $FeCl_3$ in time domain. (c) Fourier transformed amplitude spectra of input pulse and transmitted pulse in frequency domain.

3. Discussion of results

Multiple reflections of THz pulse occur between the two surfaces of sample showing small total absorption and frequency dependence of the complex amplitude of the transmitted signal $t(\omega)$ is given by [15],

$$t(\omega) = \frac{t_{12}t_{21}\,\exp(-\alpha L/2)\exp(i\beta)}{1 + r_{12}r_{21}\,\exp(-\alpha L)\exp(2i\beta)} \tag{1}$$

where t_{12}, t_{21} are complex Fresnel transmission coefficients from air-to-sample and sample-to-air of length L; r_{12}, r_{21} are the corresponding reflection coefficients; β being the modulus of propagation vector, and power absorption coefficient is given by: $\alpha = 4\pi n_i/\lambda_o$, and $\beta = 2\pi n_r L/\lambda_o$, with n_i and n_r designating the imaginary and real parts of refractive index. From this, it is possible to determine the magnitude and phase difference of $t(\omega)$. The complex spectrum $E_{ref}(\omega)$ of reference THz pulse is related to the complex spectrum $E_o(\omega)$ of output THz pulse through the equation, $E_o(\omega)/E_{ref}(\omega) = t(\omega)\exp[-i\beta_o(\omega)]$, where β_o ($=2\pi L/\lambda_o$) accounts for the air space displaced by the sample. We can numerically remove the multiple reflection effects from our measured data to determine power absorption $\alpha(\omega)$ and real part of refractive index as shown in Fig. 2(a and b) by using Fabry–Perot analysis of Eq. (1), and measure the value of $E_o(\omega)/E_{ref}(\omega)$. The power absorption shows a linear increase up to 1.7 THz, and further it increases much more rapidly with no tendency for saturation. The refractive index, on the contrary, shows frequency independent behavior in the frequency window of 0.5–2.4 THz. However, in high frequency range (from 2.4 to 3.0 THz), the refractive index decreases with increasing frequency. This is rather different with respect to the measured values of absorption and index of refraction for P3MeT-PF_6, also the dc

conductivity in both systems are different [7]. This suggests that the carrier dynamics at the nanoscopic level in MEH-PPV/$FeCl_3$ is quite different system with respect to that in P3MeT-PF_6 and PPy-PF_6. This information is quite important while using soluble PPV derivatives for various polymer electronics applications [16] and [17].

(44K)

Fig. 2. Comparison of measured data (dots) with Lorenz oscillator model (fit shown by solid line): (a) power absorption coefficient; (b) index of refraction; (c) real conductivity—the inset shows the log–log plot of σ_r vs. f, and the solid line is the power-law fit to the equation: $\ln \sigma_r(\omega) = \ln b + s \ln \omega$, where '$s$' is 2.4; (d) imaginary conductivity.

The frequency dependent dielectric response $\varepsilon(\omega)$ for semiconductors and conducting polymers is described by the general relation [15],

$$\varepsilon(\omega) = \varepsilon_{\text{poly}}(\omega) + \frac{i\sigma(\omega)}{\omega\varepsilon_o} = [n_r(\omega) + in_i(\omega)]^2, \tag{2}$$

where $\varepsilon_{\text{poly}}(\omega)$ is the dielectric constant of undoped polymer, $\sigma(\omega)$ is the complex conductivity $[\sigma(\omega) = \sigma_r(\omega) + i\sigma_i(\omega)]$ and ε_o is the free space permittivity. From the measured values of $n_r(\omega)$ and $n_i(\omega)$, real conductivity $\sigma_r(\omega)$ and imaginary conductivity $\sigma_i(\omega)$ at normal incidence $R = |(1 - n)/(1 + n)|^2$, where $n = n_r(\omega) + in_i(\omega)$, can be obtained as shown in Fig. 2 (c and d), respectively. The increasing values of $\sigma_r(\omega)$ for MEH-PPV/$FeCl_3$ samples are quite different with respect to that expected from the Drude models which has a Lorentzian line shape centered at dc.

The complex dielectric function for Drude–Lorentz oscillator (DLO) model is obtained by the combination of Drude term (second term in Eq. (3)) and localized Lorentzian oscillators (third term in Eq. (3)), as given by [11],

$$\varepsilon(\omega) = \varepsilon_{\text{poly}} - \frac{{\omega_p}^2}{\omega(\omega + i\Gamma)} - \sum_j \frac{{\Omega_{pj}}^2}{({\omega^2} - {\omega_j}^2) + i\omega\gamma_j} \tag{3}$$

where $\varepsilon_{\text{poly}}$ is the frequency independent dielectric constant; ω_j, γ_j and Ω_{pj} are the normalized harmonic oscillator frequency, spectral width, and oscillator coupling strength, respectively. The fitting parameters of Fig. 2 for the DLO model, $\omega_1/2\pi = 4$ THz, $\gamma_1/2\pi = 4$ THz, $\Omega_{p1}/2\pi = 14.7$ THz, and $\varepsilon_{\text{poly}} = 1.5^2$. The index of refraction is high value in our measured THz frequency range and the value is not saturate in high frequency range. It decreases with increasing frequency. We used the frequency independent dielectric constant of undoped polymer. Assuming one effective oscillator, the reflectance can be expressed in terms of the parameters of DLO model by using the reflectance equation [11],

$$R(\omega) = \frac{1 + |\varepsilon(\omega)| - \{2(\varepsilon_1(\omega) + |\varepsilon(\omega)|)\}^{1/2}}{1 + |\varepsilon(\omega)| + \{2(\varepsilon_1(\omega) + |\varepsilon(\omega)|)\}^{1/2}} \quad (4)$$

The above equation yields a rather good fit to the reflectance data, as shown in Fig. 3. A single Lorentz oscillator is adequate enough to obtain a good fit to the measured data, as shown in Fig. 3. Surprisingly, with and without the Drude parameters [that means $\omega_p/2\pi$ is either zero or 10 THz, and $\Gamma/2\pi$ is either 0 or 200 THz] in the DLO model, the fit remains quite identical. Hence, the contribution from second term (Drude) is negligible while compared to the third term (LO) in Eq. (3). This suggests that the free carrier contribution is too small with respect to the localized carriers in our measured frequency range. Moreover, this is understandable from the large value of the coupling constant ($\Omega_{p1}/2\pi$ = 14.7 THz) for LO indicating that the charge carriers are subjected to strong intra-chain localization, as a result the delocalized inter-chain transport that usually gives rise to the Drude term is very much subdued. Although the Drude contribution in this system is rather small, it is an essential ingredient to obtain the best fit to the data. Furthermore, this also explains why the fit with LO parameters alone do not vary after adding the Drude parameters term to the fit. Another interesting feature in the THz-TDS data of doped MEH-PPV is that, although a log–log plot of $\sigma_r(\omega)$, as shown in the inset in Fig. 2(c), yields a power law fit that is typically observed in disordered systems [13], in this case it looks like an artifact. Since the Lorentz oscillators are strongly coupled, as shown by the large value of the coupling constant, this logarithmic increase in real conductivity is due to the resonant energy absorption at THz frequencies below 4 THz, in a narrow range of frequency (the theoretical fitting curve to the real part of conductivity shows a resonant peak around 4 THz). This suggests that in doped MEH-PPV, the presence of large side groups inhibits the inter-chain transport significantly, and the intra-chain localized states are strongly coupled to each other. The absorbed energy by the oscillators mainly assists intra-chain hopping transport among the localized sites. This also explains why the Drude contribution is quite weak in case of doped MEH-PPV, unlike in case of doped PPy and P3MeT.

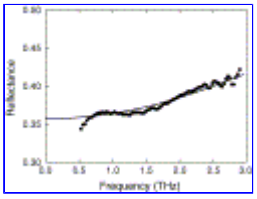

(11K)

Fig. 3. Comparison of reflectance in frequency domain. Dots are measured data and solid line is the fit to Eq. (4) in accordance with Lorenz oscillator model.

In order to understand why the THz-TDS in doped MEH-PPV is rather different from that in PPy and P3MeT, a phenomenological model for the electronic properties of doped conjugated polymers is considered in terms of inter-chain transfer integral ($t_\perp$), on-site electron–electron correlation energy (U) and amplitude of random potential (W) [18]. Typically, these three parameters are expected to play crucial role in determining the intrinsic metallic state of doped conjugated polymers. In fact, in disordered quasi-one-dimensional systems like conducting polymers, $t_\perp$ mimics the role of free carrier density, since larger $t_\perp$

implies the presence of more number of delocalized carriers and vice versa.

In typical metallic systems, with less disorder, both W and U are negligible; and as the extent of disorder increases both W and U contribute to the diffusive motion of charge carriers, and the system moves to the insulating side of MI transition. Whereas in case of $t_\perp$, it is well know that in low dimensional systems $t_\perp$ plays a significant role in MI transition (typically higher values of $t_\perp$ makes the system more metallic). In conducting polymers, a metallic state is facilitated by large $t_\perp$, and small values of W and U [18] and this, to a large extent, is achieved by the ordering of chains and morphology of the system. These guidelines are useful in understanding the THz-TDS data in various types of conducting polymers. The large side group and the solution casting process in case of MEH-PPV enhance the inter-chain separation and disorder; as a result, the values of $t_\perp$, W and U are considerably larger in case of MEH-PPV with respect to both PPy and P3MeT. The complex dielectric responses in metallic (PPy-PF_6), in (P3MET-PF_6) which is just on the insulating side of MI transition and in insulating (MEH-PPV/$FeCl_3$) follow Drude, localization-modified Drude and LO models, respectively.

4. Conclusions

In summary, the reflectance data from THz-TDS fit to LO model, since large number of carriers is strongly localized. The large value of the coupling constant indicates that the intra-chain localization is quite strong with very weak inter-chain transport due to the large side group in PPV chains and the amorphous nature of the system. A phenomenological model, in terms of $t_\perp$, U and W, is used to explain the THz-TDS response in MEH-PPV/$FeCl_3$ with respect to doped PPy and P3MeT.

Acknowledgement

Authors thank S. Ramakrishnan and G. Padmanaban for MEH-PPV samples.

References

[1] In: H.S. Nalwa, Editor, *Handbook of Organic Conductive Molecules and Polymers* **vols. 1–4**, John Wiley, New York (1997).

[2] R. Menon, C.O. Yoon, D. Moses and A.J. Heeger In: T.A. Skotheim, R. Elsenbaumer and J.R. Reynolds, Editors, *Handbook of Conducting Polymers* (second ed.), Marcel Dekker, New York (1998), p. 27.

[3] R.S. Kohlman and A.J. Epstein In: T.A. Skotheim, R. Elsenbaumer and J.R. Reynolds, Editors, *Handbook of Conducting Polymers* (second ed.), Marcel Dekker, New York (1998), p. 85.

[4] D. Grischkowsky, S. Keiding, M. van Exter and Ch. Fattinger, *J. Opt. Soc. Am. B* **7**

(1990), p. 2006.

[5] N. Katzenellenbogen and D. Grischkowsky, *Appl. Phys. Lett.* **61** (1992), p. 840.

[6] T.-I. Jeon, D. Grischkowsky, A.K. Mukherjee and R. Menon, *Appl. Phys. Lett.* **77** (2000), p. 2452.

[7] T.-I. Jeon, D. Grischkowsky, A.K. Mukherjee and R. Menon, *Appl. Phys. Lett.* **79** (2001), p. 4142.

[8] H.C.F. Martens, H.B. Brom and P.W.M. Blom, *Phys. Rev. B* **60** (1999), p. 8489.

[9] S. Karg, V. Dyakonov, M. Meier, W. Riess and G. Paasch, *Synth. Met.* **67** (1994), p. 165.

[10] G. Padmanaban and S. Ramakrishnan, *J. Am. Chem. Soc.* **122** (2000), p. 2244.

[11] A. Ugawa, G. Ojima, K. Yakushi and H. Karoda, *Phys. Rev. B* **38** (1988), p. 5122.

[12] N.W. Ashcroft and N.D. Mermin, Solid State Physics, Holt, Rinehart and Winston, New York (1976).

[13] N.F. Mott and M. Kaveh, *Adv. Phys.* **34** (1985), p. 329.

[14] M. van Exter and D. Grischkowsky, *Appl. Phys. Lett.* **56** (1990), p. 1694.

[15] M. Born and E. Wolf, Principles of Optics, Pergamon, Oxford (1987).

[16] R.H. Friend, *Nature* **397** (1999), p. 121.

[17] S.E. Shaheen, C.J. Brabec, N.S. Sariciftci, F. Padinger, T. Fromherz and J.C. Hummelen, *Appl. Phys. Lett.* **78** (2001), p. 841.

[18] H.C.F. Martens, J.A. Reedijk, H.B. Brom, D.M. de Leeuw and R. Menon, *Phys. Rev. B* **63** (2001), p. 073203.
H.C.F. Martens, H.B. Brom and R. Menon, *Phys. Rev. B* **64** (2001), p. R201102.